SCIENTIFIC REPORTS

OPEN

SUBJECT AREAS:
HETEROGENEOUS CATALYSIS
POROUS MATERIALS
FUEL CELLS
STRUCTURAL PROPERTIES

Received
20 August 2013

Accepted
3 October 2013

Published
22 October 2013

Correspondence and requests for materials should be addressed to Y.D. (yding@sdu.edu.cn)

Nanoporous gold as an active low temperature catalyst toward CO oxidation in hydrogen-rich stream

Dongwei Li[1], Ye Zhu[1], Hui Wang[1] & Yi Ding[1,2]

[1]Center for Advanced Energy Materials & Technology Research (AEMT), and School of Chemistry and Chemical Engineering, Shandong University, Jinan 250100, China, [2]Shandong Applied Research Center for Gold Technology (Au-SDARC), Yantai 264005, China.

Preferential CO oxidation (PROX) was investigated by using dealloyed nanoporous gold (NPG) catalyst under ambient conditions. Systematic investigations were carried out to characterize its catalytic performance by varying reaction parameters such as temperature and co-existence of CO_2 and H_2O, which revealed that NPG was a highly active and selective catalyst for PROX, especially at low temperature. At 20°C, the exit CO concentration could be reduced to less than 2 ppm with a turnover frequency of 4.1 × 10^{-2} s^{-1} at a space velocity of 120,000 mL h^{-1} g^{-1}_{cat}. and its high activity could retain for more than 24 hours. The presence of residual Ag species in the structure did not seem to improve the intrinsic activity of NPG for PROX; however, they contributed to the stabilization of the NPG structure and apparent catalytic activity. These results indicated that NPG might be readily applicable for hydrogen purification in fuel cell applications.

Proton exchange membrane fuel cells (PEMFCs) have been attracting much attention because of its high energy efficiency and environmental compatibility. Hydrogen as the fuel of PEMFC is traditionally produced by steam reforming, but the resulted gases always contain a small quantity of CO (0.5–2%), which poisons platinum on anode of PEMFCs. Among the popular methods for CO removal from H_2 steam, preferential CO oxidation (PROX) appears to be the most promising one[1–4]. For an ideal PROX catalyst, it should meet primarily the following key requirements: (1) high CO oxidation conversion, (2) low H_2 oxidation activity, (3) resistance to deactivation caused by CO_2 and H_2O. Considering system integration and miniaturization, it is also highly desired that the catalyst is durable at the start-up (room temperature) and operation (~80°C) temperature of PEMFCs.

Among various catalysts studied for PROX, supported gold catalysts[5–7] are found to be more active than Pt-based catalysts[8,9] and metal oxides (Cu-based catalysts)[10,11], especially at low temperature. However, it has been shown that supported gold catalysts tended to deactivate under realistic conditions because of the accumulation of carbonate-like species at the support interface[12,13]. In comparison, although no carbonate-like species were detected for unsupported gold powder (mean particle size 20 nm) by diffuse reflectance infrared Fourier transform spectroscopy[14], it was rarely active for CO oxidation.

In the past few years, dealloyed nanoporous gold (NPG) fabricated by selectively leaching less noble species (Ag, Cu or Al) from the corresponding gold alloys, has received increasing attention in catalysis[15–17], biological detection[18] and electrochemistry[19], due to its unique structural properties, such as high surface-to-volume ratio, excellent electrical and thermal conductivity, and superior chemical stability. While it has been reported that unsupported NPG can display exceptional catalytic performance for CO oxidation at low temperature[20,21], it is quite surprising that this new catalyst does not receive enough attention for gas-phase catalysis, although more recent studies have revealed very intriguing catalytic activities for NPG, such as methanol oxidative coupling[22,23], and selective benzyl alcohol oxidation[24]. To date, the catalytic properties of NPG for PROX in hydrogen stream, which is of practical significance for PEMFC development, has not been reported. Because NPG is made from a chloride-ion free dealloying process, it possesses an interesting unsupported structural feature, which is radically different from the traditional supported Au nanocatalysts. In this work we present an in-depth study on the catalytic performance of NPG for PROX.

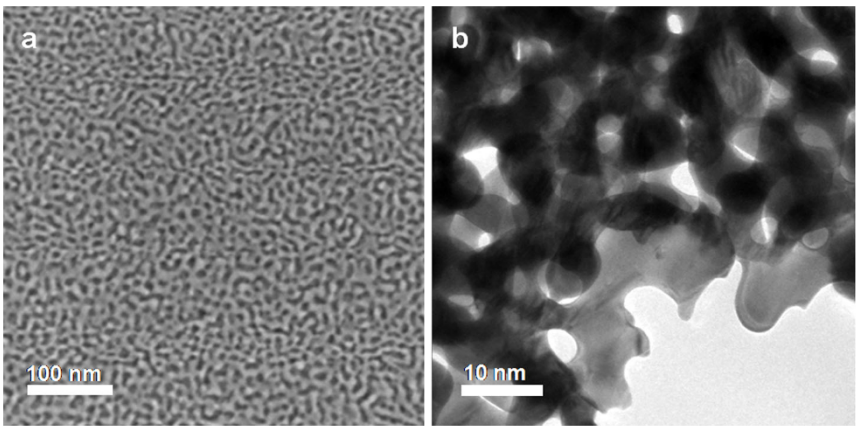

Figure 1 | **Representative SEM (a) and TEM (b) images of NPG.**

Results

Figure 1a shows a typical SEM image of NPG, which is characterized by a three dimensionally random uniform porous network structure with average ligaments around 8 nm. For clarity, the microstructure of NPG was further examined by TEM. The obvious contrast in TEM image (Figure 1b) between the dark skeletons and the inner bright regions further demonstrates the formation of interpenetrating ligament-channel structure. The open nanoporosity can be readily accessible by sources molecules in heterogeneous catalytic reactions.

For successful operation as a preferential CO oxidation catalyst in a reformer-PEMFC system, the catalyst should be capable of reducing the CO concentration from about 1% to below 50 ppm. In addition, this conversion must be achieved without the addition of excess O_2 and the competitive oxidation of H_2 must be minimized. Considering the stoichiometry between CO and O_2 in the fed gas, a selectivity of at least 50% is required for commercial operation[25]. Moreover, an efficient PROX catalyst should exhibit good performances over a wide temperature range from start-up (20°C) to typical operation temperature (80°C). We thus tested the influence of temperature on the catalytic activity of NPG for PROX, using dry gas in the absence of CO_2. As shown in Figure 2, CO conversion increased from 92.5% at 0°C to nearly 100% at 20°C, and remained at 100% till 100°C. This increased conversion was accompanied by a decrease of the selectivity, indicating higher apparent activation energy for H_2 oxidation than for CO oxidation on NPG catalysts, as often observed over supported gold catalysts[26]. At the temperature of PEMFC start-up (20°C), both conversion and selectivity could reach a perfect value, indicating that NPG was a highly active and selective catalyst toward PROX. At the temperature of PEMFC operation unit (80°C), the selectivity decreased to 60% (undesired combustion of H_2 to H_2O accounted for the remaining 40%), while the conversion still kept ~100%. NPG successfully decreased the CO concentration from 1% to less than 2 ± 1 ppm which was ideal for PEMFC application.

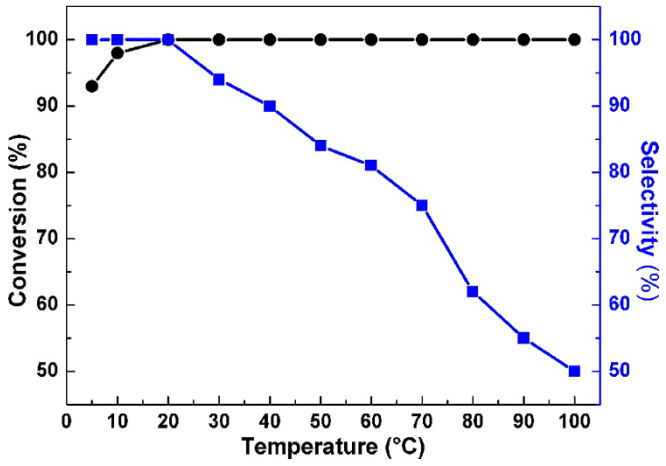

Figure 2 | **PROX in ideal reformate as a function of temperature.** Reaction condition: 1% CO, 1% O_2, 50% H_2 and N_2 balance. The space velocity is 120,000 mL h^{-1} g^{-1}_{cat}.

Table 1 lists the catalytic performance of different Au nanocatalysts for PROX. Obviously, NPG was among the best catalysts for this application. In order to further assess the catalytic activity, turnover frequency (TOF), defined as the ratio of CO_2 molecules per active site of catalyst and time, was calculated. Obviously, this TOF value is only a lower estimate because not all surface atoms are equally active for this reaction. The number of active site is determined by the density of surface atoms and the surface area of NPG catalyst. The density of surface atoms for the energetically most stable Au (111) surface is 1.4 × 10^{19} atoms/m^2, while the surface area of NPG used in this experiment was measured to be ~30 m^2 g^{-1}. TOF reported for CO oxidation on supported Au catalysts ranges from 0.034 to 0.12 s^{-1}[27]. In this study, TOF amounted to 0.16 s^{-1} at 20°C, which was strong evidence that NPG was exceptionally active for PROX.

Figure 3 shows the stability test of NPG for PROX at 20 and 80°C. The results indicated that the catalytic activity remained 100% at 20°C, and no apparent activity loss was found in 24 h. Moreover, it was found that unsupported NPG could keep a CO conversion rate of 100% for nearly 14 h at 80°C, after which the catalytic efficiency gradually decreased, and the conversion dropped to ~92% after 24 h. SEM images shown in Figure 3 (insets) clearly illustrated the structural change of NPG catalysts upon catalytic reactions. The average ligament size increased from an original value of 8 nm to about 15 nm after reaction at 20°C, and over 40 nm after reaction at 80°C. The mechanism of catalysis-induced coarsening of nanoporous metals has remained unclear to date. We speculate that the nanopore coarsening is associated with the rapid diffusion of gold atoms at chemically active surface as well as low-temperature annealing as a result of local exothermic CO oxidation.

Interestingly, in this reaction, the ligament coarsening didn't lead to obvious degeneration of the catalytic activity, especially compared with a parallel experiment where the conversion of CO oxidation in the absence of hydrogen gradually reduced after 4 h at 20°C (Figure 4). It is known that the presence of H_2 has a favourable effect on the catalytic stability of gold catalysts, either by accelerating the reaction or by preventing the catalyst deactivation, depending on the surface gold species[14,34]. For unsupported gold catalysts, H_2 has been

Table 1 | Comparison of the catalytic performance of different Au nanocatalysts for PROX

Catalyst	Preparation method	T (°C)	Conversion (%)	Selectivity (%)	Exit CO Concentration (ppm)	Ref.
Au/Al_2O_3	Impregnation	70	85	52	3000	28
Au/CeO_2	Deposition-Precipitation	40	100	51	-	29
Au/Fe_2O_3	Co-precipitation	80	99.8	51	-	30
Au/CeO_2-Al_2O_3	Impregnation	50	99	63	200	28
$Au/MnOx$-CeO_2	Deposition-Precipitation	120	90	48	-	31
Au/ZnO-TiO_2	Impregnation	80	85	43	-	32
Au/Co_3O_4-TiO_2	Impregnation	25	100	80		33
Au powder	Commercial	200	-	30	-	14
NPG	Dealloying	20	100	100	2 ± 1 (negligible)	This work
NPG	Dealloying	80	100	60	2 ± 1 (negligible)	This work

reported to activate O_2 apparently via highly oxidizing intermediate species, thus weakening the deactivation tendency[14,34].

According to the mechanism of PROX over unsupported gold powder[14], a possible mechanism with regard to this reaction over NPG is shown in Figure 5. It is believed that molecularly adsorbed O_2 is first activated on NPG by reaction with H_2 to form highly oxidative intermediates such as OOH[35,36]. Then superficial CO and intermediates react to form CO_2 and OH. The adsorbed OH would further react with superficial CO to produce CO_2 and H. The cycle is closed when two H atoms recombine into H_2 or react with O_2 molecules to form new OOH species.

Discussion

The above results indicated that NPG was a highly active and selective catalyst toward CO oxidation in ideal stream. Considering that realistic reformate in the fuel processing section contains considerable amount of H_2O (10–15%) and CO_2 (10–20%), it is therefore of practical importance to investigate whether the exceptional performance of NPG observed in ideal reformate can be maintained under more realistic conditions.

We thus evaluated the influence of CO_2 on PROX by comparing the conversion and selectivity in feed gas with and without 10% CO_2 at the temperature of PEMFC operation unit (80°C). To obtain more realistic information, here the loading of NPG catalyst was reduced to 10 mg, corresponding to a space velocity of 240,000 mL h^{-1} g^{-1}_{cat}. Figure 6a shows the effect of CO_2 on the NPG catalytic activity. It can be seen that the presence of CO_2 had slightly negative effect on CO conversion of the catalyst from about 95% in the absence of CO_2 to around 92% in the presence of CO_2, but the selectivity increased from 75 to 90%. For the catalysts of gold supported on oxides, it was reported the presence of CO_2 often inhibited the CO conversion much more seriously. In the case of Au/MnO_x for PROX, Hoflund and co-workers reported that the presence of CO_2 had a large detrimental effect on the catalytic performance, and would decrease its reactivity from 70 to 30%[37]. This inhibiting effect was often associated with the oxide support, including formation of carbonate species on the support, and chemical-state change of both active gold surface species and the oxides[38,39]. In comparison with supported Au catalysts, NPG is truly support-free and thus such deactivation can be ruled out. Moreover, the reverse water gas shift reaction has negligible effect in our system, especially at low temperature. This is why NPG is more tolerable to CO_2 as compared with supported gold catalysts. As far as the enhanced selectivity, CO_2 molecules adsorbed on the active sites might inhibit the intimate contact between hydrogen and oxygen molecules.

The effect of H_2O in the feed stream on PROX is shown in Figure 6b. H_2O was fed continuously through a syringe pump and was vaporized prior to the reaction bed, yielding ~10% water vapor in the reactant gas. Under the humidified condition, CO was still removed absolutely and the selectivity increased to 100% at 80°C. With respect to the origin of the H_2O effect, the possibility of water gas shift reaction (WGSR) can be ruled out, because a separate WGSR (1% CO + 10% H_2O) on NPG showed no CO_2 formation at the corresponding temperature. The increased selectivity could be attributed to the reaction equilibrium for H_2 oxidation, which shifted to the left in the presence of H_2O. The second reason might be related to the adsorption of H_2O molecules which led to the formation of

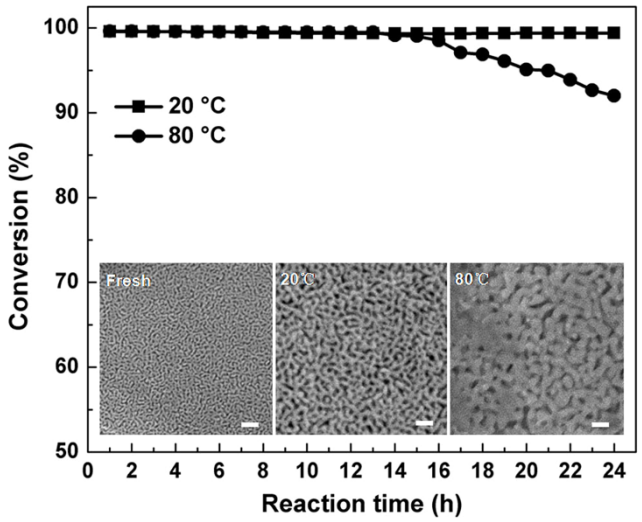

Figure 3 | The stability of NPG for PROX at 20°C (■) and 80°C (●). Insets are SEM images of NPG samples before and after catalytic reactions. Scale bars: 100 nm.

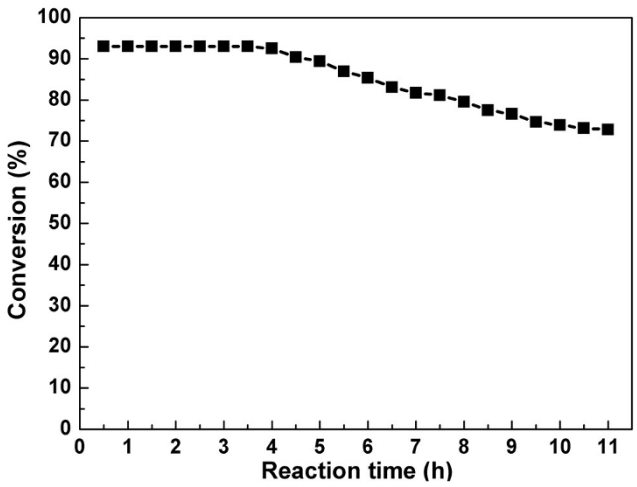

Figure 4 | Catalytic performance of NPG for CO oxidation at 20°C. The reaction gas composition: 1% CO, 10% O_2 and N_2 balance. The space velocity is 120,000 mL h^{-1} g^{-1}_{cat}.

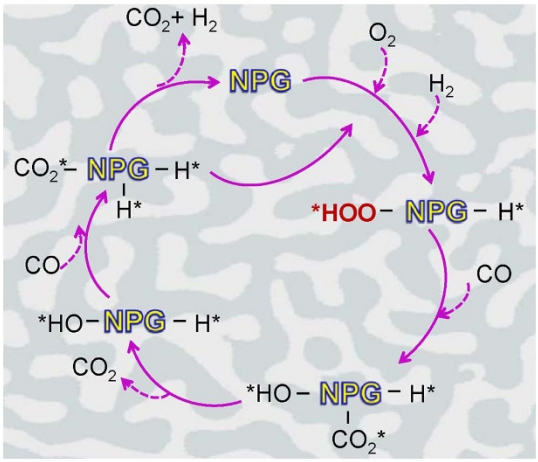

Figure 5 | **Reaction mechanism of CO oxidation in the presence of H_2 over NPG.**

carboxyl group that accelerated the adsorption of oxygen to oxidize CO into CO_2[40,41]. Figure 6c depicts the influence of co-presence of 10% CO_2 and 10% H_2O in the feed stream on PROX over NPG catalyst. Very apparently, feeding both CO_2 and H_2O in the stream has remarkably positive effect on CO removal. The CO conversion was nearly perfect and the selectivity increased from 75 to 100% at 80°C. The variation of CO conversion and selectivity with reaction time in different feed gases can be more clearly appreciated in a designed experiment as illustrated in Figure 6d. During the first 30 min, NPG catalysts behaved quite normal as observed in Figure 6a–c, with a conversion slightly over 95% and selectivity around 75%. During the second stage, 10% CO_2 was added into the stream, which slightly reduced the conversion to about 92%. After another 30 min (stage 3), 10% H_2O was introduced into the stream, which immediately increased the conversion from 92 to nearly 100%. And over the entire reaction period, continuous increase of selectivity was observed, indicating a favorable effect from the presence of H_2O and/or CO_2.

Regarding the possible contribution of silver to gold catalysis, Mou and co-workers reported that AuAg alloy particles on mesoporous supports possessed much higher activity for low temperature CO oxidation as compared to monometallic Au catalyst[42]. Considering that some silver atoms might be trapped within the ligaments of NPG during dealloying, a question often arises as whether the apparent catalytic activity is solely from NPG itself or the residual Ag atoms play an important role. In deed, several groups have noted the effect of the residual elements on CO oxidation and methanol oxidation[43,44]. For example, Bäumer and co-workers considered NPG catalyst as a bimetallic catalyst rather than a pure Au catalyst, and the superior catalytic activity for low temperature CO oxidation was attributable to the residual Ag[45]. To investigate the possible effect of Ag in the present system, control experiments were performed

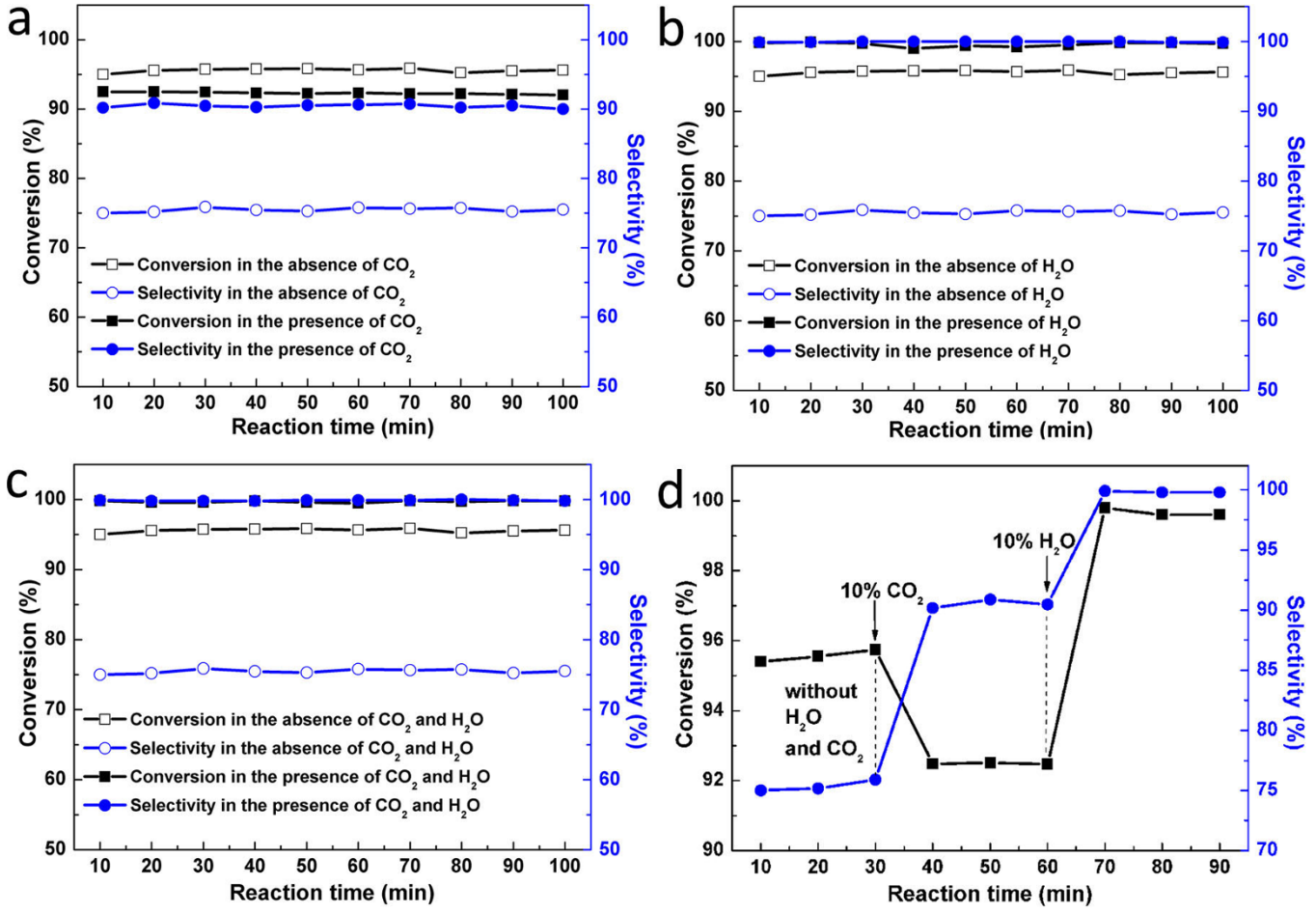

Figure 6 | (a) Effect of CO_2 on PROX over NPG at 80°C. Reaction condition: 1% CO, 1% O_2, 50% H_2, 10% CO_2 and N_2 balance. (b) Effect of H_2O on PROX over NPG at 80°C. Reaction condition: 1% CO, 1% O_2, 50% H_2, 10% H_2O and N_2 balance. (c) Effect of co-adding CO_2 and H_2O in the feed gas on PROX. Reaction condition: 1% CO, 1% O_2, 50% H_2, 10% CO_2, 10% H_2O and N_2 balance. (d) Variation of PROX with reaction time in different feed gases. Conversion (■ □); Selectivity (● ○). The space velocity is 240,000 mL h^{-1} g^{-1}_{cat}.

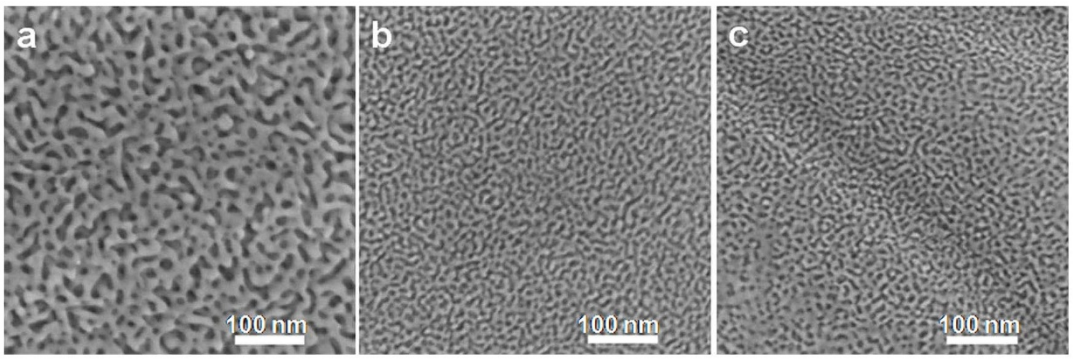

Figure 7 | SEM images of different NPG samples formed by dealloying for 260 s (a), 900 s (b), and 1800 s (c).

using NPG catalysts with different Ag contents. The residual Ag contents in the NPG catalysts were controlled by varying the dealloying period. Figure 7 shows the SEM images of NPG formed by dealloying for 260, 900, and 1800 s, from which the corresponding ligament sizes of 12, 8, and 8 nm could be observed, respectively. The residual Ag contents were measured to be 50.2, 5.3, 0.99 at. %.

Figure 8 illustrates the performance of CO oxidation and PROX over these nanoporous AuAg alloy catalysts at 20°C. It is obvious that the catalytic activity of NPG in these reactions was remarkably improved as the Ag content decreased. This is somewhat in agreement with a recent work reported by Baümer and co-workers who observed that the catalytic activity of NPG containing Ag decreased with the increase of surface Ag contents in gas-phase methanol oxidation[22]. Although our present study suggested that the residual Ag atoms in NPG catalysts did not seem to favor the observed activity, there is still no clear answer as whether Ag species can tune the catalytic properties of neighboring Au atoms when their content is sufficiently low[46].

Recently, Chen and co-workers provided nice atomic scale microscopic evidences that residual Ag could stabilize the low-coordinated surface gold sites, and these active sites were mainly responsible for the high catalytic activity of NPG for various reactions[47]. To verify this effect, we investigated the effect of residual Ag on the stability of NPG toward CO oxidation and PROX. Figure 9 shows the CO conversion at room temperature versus time in two different streams for NPG-900 and NPG-1800. While NPG-1800 exhibited higher conversion than NPG-900 under both conditions, the overall stability was evidently higher for NPG with higher Ag contents (NPG-900).

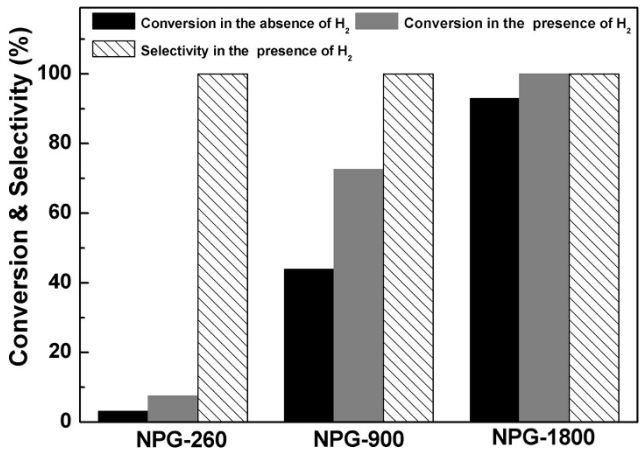

Figure 8 | Catalytic activity of different NPG samples for CO oxidation and PROX at 20°C. Reaction condition: 1% CO, 10% O_2 and N_2 balance (CO oxidation); 1% CO, 1% O_2, 50% H_2 and N_2 balance (PROX). The space velocity is 120,000 mL h^{-1} g^{-1}_{cat}.

Figure 10 shows the SEM images of NPG samples after catalytic reactions. The ligament size of NPG-1800 was obviously increased (Figure 10a, c), and the coarsening of the nanostructure decreased the surface area, thereby degrading the overall catalytic performance of CO oxidation in the absence of hydrogen. In contrast, the structure coarsening of NPG-900 was significantly retarded (Figure 10b, d) regardless of being in CO oxidation or PROX. These results provided further evidence that the presence of residual Ag species might contribute to the stabilization of the NPG structure.

In summary, NPG was found to be highly active and selective for PROX especially at low temperature, where the conversion and selectivity could reach a perfect value. Although the presence of CO_2 had slight negative influence on CO conversion, both CO_2 and H_2O enhanced the selectivity obviously. Additionally, the presence of residual Ag atoms did not seem to favor the intrinsic activity of NPG for PROX, but stabilized the apparent catalytic activity and nanostructure of NPG. It is noteworthy that, although our results suggested that the residual Ag atoms in NPG catalysts did not contribute to the observed activity, this research could still not exclude a possibility that Ag species could tune the catalytic properties of neighboring Au atoms when their content was sufficiently low. These results indicate that NPG might be readily applicable for hydrogen purification in fuel cell applications.

Methods

Catalyst preparation. NPG catalysts were fabricated by selectively etching Ag from 25 μm thick AuAg alloy (29 : 71, at. %) in concentrated nitric acid (67%). This

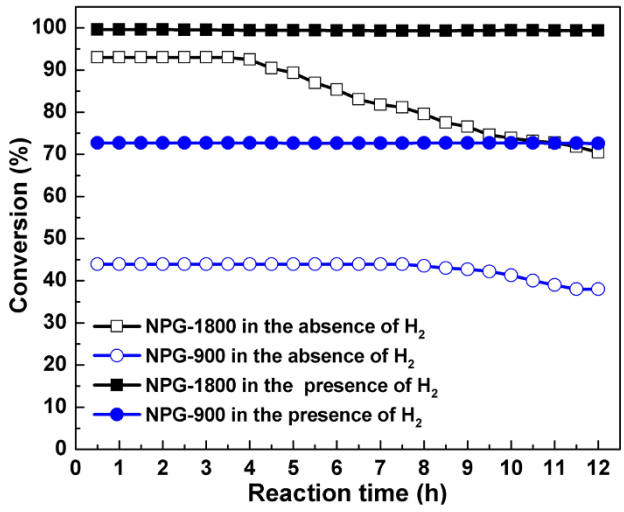

Figure 9 | CO oxidation and PROX at room temperature versus time on stream for NPG with different Ag contents. Reaction condition: 1% CO, 10% O_2 and N_2 balance (CO oxidation); 1% CO, 1% O_2, 50% H_2 and N_2 (PROX). The space velocity is 120,000 mL h^{-1} g^{-1}_{cat}.

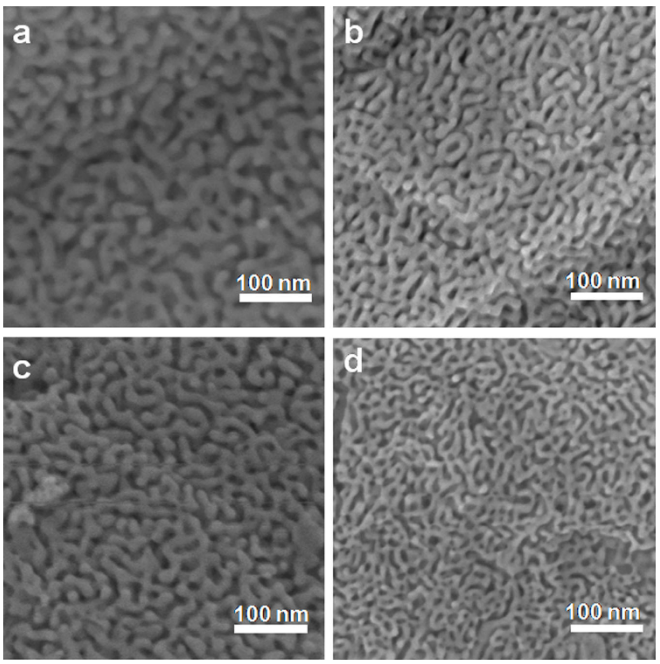

Figure 10 | SEM images of different NPG samples after catalytic reaction. (a). NPG-1800 (CO oxidation) (b). NPG-900 (CO oxidation) (c). NPG-1800 (PROX) (d). NPG-900 (PROX).

dealloying process was carried out in a standard three-electrode cell with a CHI 760C potentiostat under an applied voltage (0.4 V) at room temperature, using platinum electrode as the counter electrode and saturated calomel electrode (RHE) as the reference electrode. Before dealloying, AuAg alloy foils were annealed at 850°C for 16 h and subsequently degreased by sonicating in ethanol and rinsed with distilled water. The residual Ag contents in NPG catalysts were controlled by varying dealloying period. All NPG samples were filtered out and thoroughly washed with distilled water until no acid was detected in the filtrate, and then dried in a vacuum desiccator at room temperature.

Catalyst characterization. The microstructure of samples was characterized with a JEOL JSM-6700F field emission scanning electron microscope (SEM), equipped with an Oxford INCA x-sight energy-dispersive spectrometer (EDS) for compositional analysis. The surface area was measured with Quadrasorb SI-MP (Quantachrome Instruments) using the BET method.

Catalytic test. In all experiments, NPG catalysts were (20 mg) crushed into powder and then diluted with 0.5 g quartz sand (1-μm) to ensure adequate contact between gas reactants and the catalysts. The mixed catalysts were placed into a 4-mm-i.d. quartz tube and tested in a continuous flow fixed bed micro-reactor at atmospheric pressure. With regard to the temperature control during testing, the reactor was settled in a cold trap at 0°C and in a heating furnace at higher temperatures to keep isothermal. The reactant gas containing 1% CO, 1% O_2, 50% H_2, and N_2 for balance was guided into the reactor with a space velocity of 120,000 mL h^{-1} g^{-1}_{cat} (the typical composition in reforming stream is 45–75% H_2, 10–20% CO_2, 0.5–2% CO, and H_2O). The effect of CO_2 and H_2O was investigated, at separate runs, with addition of 10% in the respective feed gas. The amounts of CO and CO_2 were measured by an on-line infrared gas analyzer (Gasboard-3121, China Wuhan Cubic Co.). The resolution of this analyzer is 1 ppm. O_2 was analyzed by an online Shimadzu Type gas chromatograph (GC-14C) equipped with a thermal conductivity detector (TCD), using 5 Å Molecular Sieve.

CO conversion was calculated based on CO_2 formation as follows:

$$conversion\% = \frac{[CO_2]_{out}}{[CO]_{in}} \times 100\%$$

When 10% CO_2 was added in the reactant gases, the CO conversion was calculated based on CO consumption, considering otherwise possible errors in the quantification of small changes in CO_2 concentration. The selectivity was calculated from the oxygen mass balance as follows:

$$selectivity\% = \frac{0.5([CO]_{in} - [CO]_{out})}{[O_2]_{in} - [O_2]_{out}} \times 100\%$$

1. Potemkin, D. I. *et al.* Preferential CO oxidation over bimetallic Pt–Co catalysts prepared via double complex salt decomposition. *Chem. Eng. J.* **207–208**, 683–689 (2012).
2. Alayoglu, S., Nilekar, A. U., Mavrikakis, M. & Eichhorn, B. Ru–Pt core–shell nanoparticles for preferential oxidation of carbon monoxide in hydrogen. *Nat. Mater.* **7**, 333–338 (2008).
3. Park, E. D., Lee, D. & Lee, H. C. Recent progress in selective CO removal in a H_2-rich stream. *Catal. Today* **139**, 280–290 (2009).
4. Nilekar, A. U., Alayoglu, S., Eichhorn, B. & Mavrikakis, M. Preferential CO oxidation in hydrogen: reactivity of core-shell nanoparticles. *J. Am. Chem. Soc.* **132**, 7418–7428 (2010).
5. Naknam, P., Luengnaruemitchai, A. & Wongkasemjit, S. Au/ZnO and Au/ZnO-Fe_2O_3 prepared by deposition-precipitation and their activity in the preferential oxidation of CO. *Energy Fuels* **23**, 5084–5091 (2009).
6. Tu, Y. B., Luo, J. Y., Meng, M., Wang, G. & He, J. J. Ultrasonic-assisted synthesis of highly active catalyst Au/MnO_x–CeO_2 used for the preferential oxidation of CO in H_2-rich stream. *Int. J. Hydrogen Energy* **34**, 3743–3754 (2009).
7. Shodiya, T., Schmidt, O., Peng, W. & Hotz, N. Novel nano-scale Au/a-Fe_2O_3 catalyst for the preferential oxidation of CO in biofuel reformate gas. *J. Catal.* **300**, 63–69 (2013).
8. Liu, K., Wang, A. Q. & Zhang, T. Recent advances in preferential oxidation of CO reaction over platinum group metal catalysts. *ACS Catal.* **2**, 1165–1178 (2012).
9. Xu, J. *et al.* Mechanistic study of preferential CO oxidation on a Pt/NaY zeolite catalyst. *J. Catal.* **287**, 114–123 (2012).
10. Varghese, S. *et al.* CO oxidation and preferential oxidation of CO in the presence of hydrogen over SBA-15-templated CuO-Co_3O_4 catalysts. *Appl. Catal. A: Gen.* **443–444**, 161–170 (2012).
11. Gamarra, D. *et al.* Preferential oxidation of CO in excess H_2 over CuO/CeO_2 catalysts: Characterization and performance as a function of the exposed face present in the CeO_2 support. *Appl. Catal. B: Environ.* **130–131**, 224–238 (2013).
12. Wang, H. *et al.* Deactivation of a Au/CeO_2–Co_3O_4 catalyst during CO preferential oxidation in H_2-rich stream. *J. Catal.* **264**, 154–162 (2009).
13. Kim, C. H. & Thompson, L. T. Deactivation of Au/CeO_x water gas shift catalysts. *J. Catal.* **230**, 66–74 (2005).
14. Quinet, E. *et al.* H_2-induced promotion of CO oxidation over unsupported gold. *Catal. Today* **138**, 43–49 (2008).
15. Ding, Y. & Chen, M. W. Nanoporous metals for catalytic and optical applications. *MRS Bull.* **34**, 569–576 (2009).
16. Zhang, X. M. & Ding, Y. Unsupported nanoporous gold for heterogeneous catalysis. *Catal. Sci. Technol.* DOI: 10.1039/C3CY00241A (2013).
17. Asao, N. *et al.* Nanostructured materials as catalysts: nanoporous-gold-catalyzed oxidation of organosilanes with Water. *Angew. Chem. Int. Ed.* **49**, 10093–10095 (2010).
18. Yu, F. *et al.* Simultaneous Excitation of Propagating and Localized Surface Plasmon Resonance in Nanoporous Gold Membranes. *Anal. Chem.* **78**, 7346–7350 (2006).
19. Zhang, J. T., Liu, P. P., Ma, H. Y. & Ding, Y. Nanostructured porous gold for methanol electro-oxidation. *J. Phys. Chem. C* **111**, 10382–10388 (2007).
20. Zielasek, V. *et al.* Gold catalysts: nanoporous gold foams. *Angew. Chem. Int. Ed.* **45**, 8241–8244 (2006).
21. Xu, C. X. *et al.* Low temperature CO oxidation over unsupported nanoporous gold. *J. Am. Chem. Soc.* **129**, 42–43 (2007).
22. Wittstock, A., Zielasek, V., Biener, J., Friend, C. M. & Bäumer, M. Nanoporous gold catalysts for selective gas-phase oxidative coupling of methanol at low temperature. *Science* **327**, 319–322 (2010).
23. Kosuda, K. M., Wittstock, A., Friend, C. M. & Bäumer, M. Oxygen-mediated coupling of alcohols over nanoporous gold catalysts at ambient pressures. *Angew. Chem. Int. Ed.* **51**, 1698–1701 (2012).
24. Han, D. Q., Xu, T. T., Su, J. X., Xu, X. H. & Ding, Y. Gas-phase selective oxidation of benzyl alcohol to benzaldehyde with molecular oxygen over unsupported nanoporous gold. *ChemCatChem* **2**, 383–386 (2010).
25. Landon, P. *et al.* Selective oxidation of CO in the presence of H_2, H_2O and CO_2 via gold for use in fuel cells. *Chem. Comm.* 3385–3387 (2005).
26. Bamwenda, G. R., Tsubota, S., Nakamura, T. & Haruta, M. The influence of the preparation methods on the catalytic activity of platinum and gold supported on TiO_2 for CO oxidation. *Catal. Lett.* **44**, 83–87 (1997).
27. Kandoi, S., Gokhale, A. A., Grabow, L. C., Dumesic, J. A. & Mavrikakis, M. Why Au and Cu are more selective than Pt for preferential oxidation of CO at low temperature. *Catal. Lett.* **93**, 93–100 (2004).
28. Fonseca, J. *et al.* Preferential CO oxidation over nanosized gold catalysts supported on ceria and amorphous ceria–alumina. *Appl. Catal. B: Environ.* **128**, 10–20 (2012).
29. Sakwarathorn, T., Luengnaruemitchai, A. & Pongstabodee, S. Preferential CO oxidation in H_2-rich stream over Au/CeO_2 catalysts prepared via modified deposition–precipitation. *J. Ind. Eng. Chem.* **17**, 747–754 (2011).
30. Landon, P. *et al.* Selective oxidation of CO in the presence of H_2, H_2O and CO_2 utilising Au/a-Fe_2O_3 catalysts for use in fuel cells. *J. Mater. Chem.* **16**, 199–208 (2006).
31. Tu, Y. B. *et al.* CO preferential oxidation over Au/MnOx–CeO_2 catalysts prepared with ultrasonic assistance: Effect of calcination temperature. *Fuel Process. Technol.* **93**, 78–84 (2012).
32. Chen, Y. W., Lee, D. S. & Chen, H. J. Preferential oxidation of CO in H_2 stream on Au/ZnO-TiO_2 catalysts. *Int. J. Hydrogen Energy* **37**, 15140–15155 (2012).
33. Chen, Y. W., Chen, H. J. & Lee, D. S. Au/Co_3O_4–TiO_2 catalysts for preferential oxidation of CO in H_2 stream. *J. Mol. Catal. A: Chem.* **363–364**, 470–480 (2012).

34. Rossignol, C. *et al*. Selective oxidation of CO over model gold-based catalysts in the presence of H_2. *J. Catal.* **230**, 476–483 (2005).
35. Quinet, E. *et al*. On the mechanism of hydrogen-promoted gold-catalyzed CO oxidation. *J. Catal.* **268**, 384–389 (2009).
36. Déronzier, T., Morfin, F., Massin, L., Lomello, M. & Rousset, J. L. Pure nanoporous gold powder: synthesis and catalytic properties. *Chem. Mater.* **23**, 5287–5289 (2011).
37. Hoflund, G. B., Gardner, S. D., Schryer, D. R., Upchurch, B. T. & Kielin, E. J. Effect of COz on the performance of Au/lMnO, and Pt/SnO, low-temperature CO oxidation catalysts. *Langmuir* **11**, 3431–3434 (1995).
38. Avgouropoulos, G. *et al*. A comparative study of Pt/γ-Al_2O_3, Au/α-Fe_2O_3 and CuO–CeO_2 catalysts for the selective oxidation of carbon monoxide in excess hydrogen. *Catal. Today* **75**, 157–167 (2002).
39. Schubert, M. M., Venugopal, A., Kahlich, M. J., Plzak, V. & Behm, R. J. Influence of H_2O and CO_2 on the selective CO oxidation in H_2-rich gases over Au/α-Fe_2O_3. *J. Catal.* **222**, 32–40 (2004).
40. Daté, M., Okumura, M., Tsubota, S. & Haruta, M. Vital role of moisture in the catalytic activity of supported gold nanoparticles. *Angew. Chem. Int. Ed.* **43**, 2129–2132 (2004).
41. Bongiorno, A. & Landman, U. Water-enhanced catalysis of CO oxidation on free and supported gold nanoclusters. *Phys. Rev. Lett.* **95**, 106102 (2005).
42. Wang, A. Q., Liu, J. H., Lin, S. D., Lin, T. S. & Mou, C. Y. A novel efficient Au–Ag alloy catalyst system: preparation, activity, and characterization. *J. Catal.* **233**, 186–197 (2005).
43. Wang, L. C., Zhong, Y., Widmann, D., Weissmüller, J. & Behm, R. J. On the nature of active sites on nanoporous Au catalysts for CO oxidation: a combined micro-reactor and TAP reactor study. *ChemCatChem* **4**, 251–259 (2012).
44. Moskaleva, L. V. *et al*. Silver residues as a possible key to a remarkable oxidative catalytic activity of nanoporous gold. *Phys. Chem. Chem. Phys.* **13**, 4529–4539 (2011).
45. Wittstock, A. *et al*. Nanoporous Au: An unsupported pure gold catalyst? *J. Phys. Chem. C* **113**, 5593–5600 (2009).
46. Röhe, S. *et al*. CO oxidation on nanoporous gold: a combined TPD and XPS study of active catalysts. *Surf. Sci.* **609**, 106–112 (2013).
47. Fujita, T. *et al*. Atomic origins of the high catalytic activity of nanoporous gold. *Nat. Mater.* **11**, 775–780 (2012).

Acknowledgments

This work was sponsored by the National 973 Program Project of China (2012CB932800), and the National Science Foundation of China (51171092) and the Research Fund for the Doctoral Program of Higher Education of China (20090131110019).

Author contributions

Y.D. and D.L. designed this research; D.L. carried out the experiments and analyzed the data; Y.Z. and H.W. contributed to the discussion; D.L. and Y.D. wrote the paper.

Additional information

Competing financial interests: The authors declare no competing financial interests.

How to cite this article: Li, D.W., Zhu, Y., Wang, H. & Ding, Y. Nanoporous gold as an active low temperature catalyst toward CO oxidation in hydrogen-rich stream. *Sci. Rep.* **3**, 3015; DOI:10.1038/srep03015 (2013).